photonics

MDPI

Article

Stable Bound States in the Continuum Resonances Enabled by Hetero-Material out of Plane Asymmetry Metasurface

Zhang Guoshuai [1,2,*], Zheng Yi [1], Jiang Xiaowei [1,2] and Zhan Chunlian [2]

[1] College of Information Engineering, Quzhou College of Technology, Quzhou 324000, China; 18157031307@163.com (Z.Y.); josephjiangquzhi@126.com (J.X.)
[2] College of Optical and Electronic Technology, China Jiliang University, Hangzhou 310018, China; zc913@163.com
* Correspondence: zgsh19881207@126.com

Abstract

SP-QBIC resonances are highly sensitive to asymmetry parameters. Meanwhile, achieving polarization-wavelength-stable QBIC resonances in metasurfaces remains challenging. To address these issues, this study proposes hetero-material out-of-plane (HOP) metasurfaces. First, the influence of the asymmetry parameter on the resonance spectra of the HOP asymmetric metasurfaces (AMS) is analyzed. Compared with in-plane (IP) AMS, the QBIC resonance wavelength of the HOP AMS remains essentially stable as the asymmetry parameter varies, and both the resonance linewidth and the quality (Q) factor exhibit stronger robustness—especially when the hetero-material is located up the symmetric metasurface (HOP_u). Second, the effect of the refractive index of the hetero-material n_l on the resonance spectra of the HOP_u AMS and (the hetero material is located below the symmetric metasurface) HOP_b AMS is investigated. As the n_l increases, the QBIC resonance wavelengths of HOP AMS red-shift; meanwhile, the Q factor of the HOP_u gradually decreases, whereas that of the HOP_b AMS remains almost unchanged. Simulations reveal that HOP AMS resonances exhibit strong robustness against device fabrication errors. Finally, by varying the incident light polarization angle, it is verified that the proposed HOP AMS enables excitation polarization wavelength stable QBIC resonance. The multipole decomposition elucidates the physical mechanism by which HOP AMS can excite polarization wavelength stable SP-QBIC resonances. The key structural parameters of the HOP AMS for exciting polarization wavelength stable SP-QBIC resonance were confirmed. This study provides a theoretical foundation for designing and fabricating metasurfaces that support resonance stable and polarization wavelength stable QBIC resonances.

Keywords: bound states in the continuum; polarization wavelength stable; hetero-material out-of-plane; metasurface

Check for updates

Received: 28 July 2026
Revised: 7 September 2026
Accepted: 9 September 2026
Published: 15 September 2026

Copyright: © 2026 by the authors. Licensee MDPI, Basel, Switzerland. This article is an open access article distributed under the terms and conditions of the Creative Commons Attribution (CC BY) license.

1. Introduction

Bound states in the continuum (BICs) were first proposed by Neumann and Wigner in quantum mechanics [1], and through continuous enrichment and exploration of their physical mechanisms, they have gradually been applied in optical systems [2,3]. BICs are a type of radiation-free localized state that can maintain perfect confinement even within the continuous region of the radiation zone, possessing infinite lifetime [4,5]. BICs have attracted widespread attention due to their unique physical characteristics and superior performance metrics. Since BICs have no radiation channels, they are all dark modes and

the energy output to the environment is theoretically zero. For practical applications, it is necessary to convert BICs into quasi-BICs (QBICs) with high quality (Q) factors [6,7]. QBICs have been widely applied in fields such as low-threshold lasers [8,9], Goos-Hänchen effect enhancement [10,11], luminescence enhancement [12,13], and highly sensitive sensors [14,15].

Currently, there are two main methods to convert BICs into QBICs: breaking the symmetry of micro-nano structures [16,17] and causing destructive interference of radiation by adjusting micro-nano structural parameters [18,19]. The method of obtaining symmetry-protected (SP) QBICs by breaking micro-nano structural symmetry is not only simple and efficient, but also offers good scalability in the operating wavelength of SP-QBICs, as only the geometric dimensions of the micro-nano structures need to be adjusted for the desired operating wavelength. Therefore, obtaining SP-QBICs resonance by breaking micro-nano structural symmetry has become the preferred method, with breaking the in-plane geometric symmetry being the more mainstream approach at present. Although obtaining SP-QBIC resonance by breaking micro-nano structural symmetry has the aforementioned advantages; however, there is an unavoidable problem. The resonance wavelength and Q factor of SP-QBIC resonance are extremely sensitive to the asymmetry parameters of micro-nano structures [20–22]. When geometric asymmetry parameters undergo slight deviations, the resonance wavelength and Q factor change dramatically, imposing high requirements on the fabrication technology of micro-nano structures. To improve the robustness of SP-QBIC resonance against asymmetry parameter variations and reduce the fabrication difficulty of micro-nano structures, various research teams have successively proposed solutions. To achieve stability of SP-QBIC resonance wavelength with variations in asymmetry parameters, translation-asymmetric metasurfaces and volume-compensated asymmetric metasurfaces are proposed [23,24]. Theoretical and experimental results have demonstrated that both methods can improve the stability of the SP-QBIC resonance wavelength. In order to enhance the robustness of SP-QBIC resonance Q factor against asymmetric parameter variations. Liang and Huang et al. respectively achieved robustness enhancement of SP-QBIC resonance Q factor based on topological BICs and the weak eigenfield method [25,26]. Although the aforementioned methods can effectively achieve stability of either SP-QBIC resonance wavelength or Q factor, but they cannot simultaneously achieve stability of both SP-QBIC resonance wavelength and Q factor.

To simultaneously enhance the robustness of both the resonance wavelength and the Q factor of SP-QBICs against asymmetry parameters, out-of-plane (OP) asymmetric nanostructures have recently been introduced [27,28]. Wu et al. demonstrated that OP asymmetric metasurfaces can significantly improve the stability of the SP-QBIC resonance wavelength and Q factor. However, the robustness of the Q factor still needs to be improved [27]. To further increase the robustness of the Q factor, Wang and Sun et al. proposed placing a hetero- material above the meta-atoms, forming a hetero- material out-of-plane (HOP) asymmetric metasurface (AMS). Both theoretical and experimental results show that SP-QBICs excited by HOP AMS exhibit markedly improved wavelength and Q factor stability [29,30]. Despite these advances, two critical issues remain. First, the influence of hetero-material key parameters on SP-QBIC resonances has rarely been investigated. Second, HOP AMS reported so far cannot excite polarization wavelength stable SP-QBIC resonances (the SP-QBIC resonance wavelength remaining stable as the polarization angle varies), restricting design flexibility and limiting potential applications.

To this end, this study proposes HOP AMS capable of achieving polarization wavelength stable SP-QBIC resonances. Based on HOP AMS, the influence of key structural parameters of hetero-material on SP-QBIC resonance is explored, and the physical mechanism by which HOP AMS can excite SP-QBIC resonance is investigated. The specific

conditions under which HOP AMS can excite polarization wavelength stable SP-QBIC resonances are studied. The underlying physical mechanism enabling it to excite polarization wavelength stable SP-QBIC resonances is explored. The research in this study provides a theoretical foundation for the design and fabrication of HOP AMS with strong robustness and polarization wavelength stability.

2. Models and Methods

Figure 1 shows the structure diagram of dielectric metasurface. As shown in Figure 1, the dielectric metasurface consists of periodically arranged rectangular microstructure meta-atoms. Figure 1a shows the top view of a completely symmetric dielectric metasurface structure, where the periods in the x- and y-axis directions are $P_x = P_y = P = 40$ μm, respectively. The rectangular microstructure meta-atoms have width and length of $w = 6$ μm and $L = 22.32$ μm, respectively. Under these structural parameters, the metasurface can excite an SP-QBIC resonance at approximately 6.8 THz (44 μm). Metasurfaces operating in this band can be applied in terahertz laser, terahertz spectral sensing and related fields. The meta-atom and metasurface substrate materials are silicon (refractive index $n_s = 3.42$) and silicon dioxide (refractive index 1.45), respectively, and the metasurface substrate thickness is $t = 8$ μm. Figure 1b–d correspond to the hetero-material located up the symmetric metasurface (HOP_u), the hetero-material located below the symmetric metasurface (HOP_b), and the in-plane (IP) AMS, respectively. As seen in Figure 1b,c, the rectangular nanorod meta-atom thickness is $h_t = 9$ μm, and the gap between meta-atoms is $g = 4.8$ μm. The hetero-material thickness and refractive index for HOP_u and HOP_b asymmetric metasurfaces are h_l and n_l, respectively. The IP asymmetric metasurface contains meta-atoms with refractive index n in addition to silicon meta-atoms. The IP metasurface maintains in-plane symmetry when $n = n_s$. The asymmetric parameters for HOP and IP AMS are $\alpha = h_l/h_t$ and $\alpha_\varepsilon = (n_s - n)/n_s$, respectively.

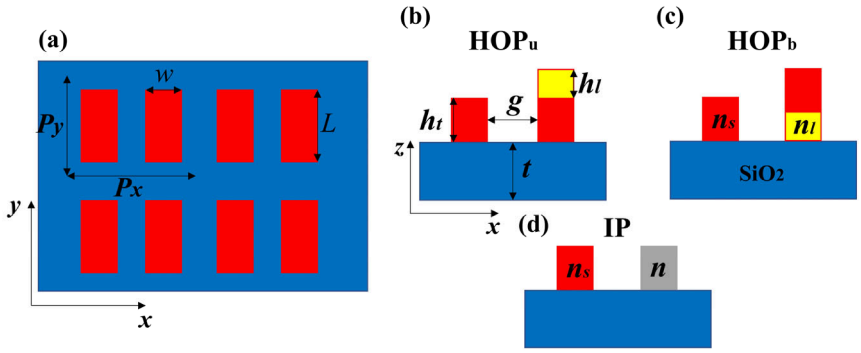


Figure 1. Dielectric metasurface. (**a**) All-dielectric metasurface; (**b**) HOP_u AMS; (**c**) HOP_b AMS; (**d**) IP AMS.

Current micro-nanofabrication technologies are fully capable of meeting the fabrication requirements for the HOP and IP asymmetric metasurfaces shown in Figure 1 [31,32]. Take HOP_u AMS as an example. Initially, a SiO_2 layer of the required thickness is deposited onto a customized SOI chip. Next, a photoresist is spin-coated on the SiO_2 film, and electron beam lithography is performed. A Cr hard mask layer is deposited via electron beam evaporation and lifted off, and reactive ion etching is employed to etch the SiO_2 film to create hetero-material rectangular meta-atoms. Then, the photoresist is spin-coated, electron beam lithography is performed, a Cr hard mask layer is deposited and lifted off, and reactive ion etching is employed to etch the Si film to form Si rectangular meta-atoms. Finally, the hard mask layer is removed to obtain the desired HOP_u AMS.

The optical characteristics of the metasurfaces are simulated using finite difference time domain method. Periodic boundary conditions are applied in the x and y directions, and perfectly matched layer boundary conditions are applied in the z direction. The incident light wave with electric field along the y-direction (incident light polarization angle $\Phi = 90^\circ$, transverse magnetic mode, TM) is normally incident onto the metasurface along the z-direction. Figure 2a shows the three-dimensional band diagram of the dielectric metasurface (Figure 1a) under TM polarization. The eigenwavelength at the Γ point is 44.3 μm. The three-dimensional Q factor and far-field polarization state in momentum space are specifically shown in Figure 2b,c. In Figure 2b,c, the Q factor tends to infinity at the Γ point, and the far-field polarization state exhibits a distinct vortex center. The above results indicate that the BIC formed by the dielectric metasurface is a symmetry-protected BIC. By breaking the structural symmetry of the metasurface, the symmetry-protected BIC can be converted into a high-Q SP-QBIC resonance.

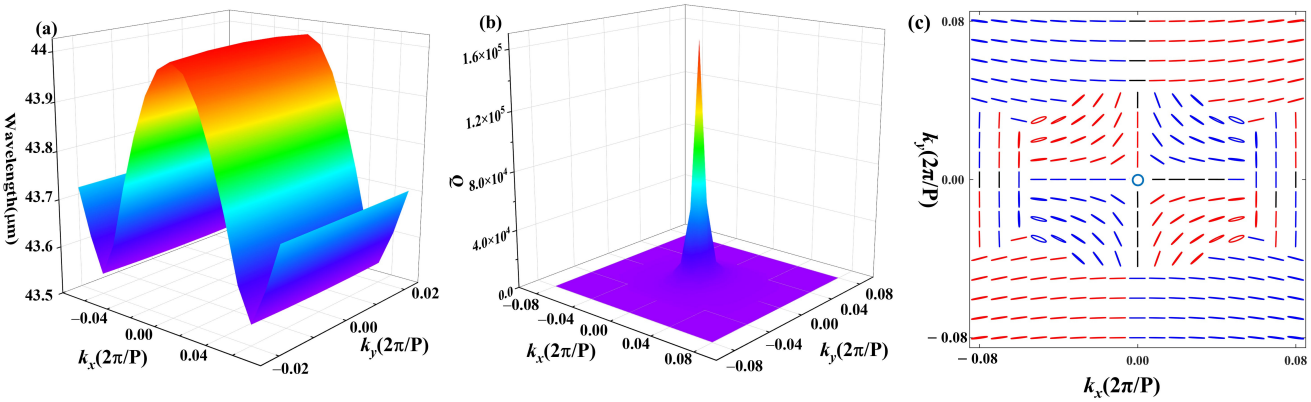


Figure 2. The band structures, Q factor and far-field polarization states of all-dielectric symmetry metasurface (g = 4.8 μm) (**a**) Band structures; (**b**) Q factor; (**c**) the distribution of far-field polarization states.

To investigate the effects of different symmetry-breaking strategies on QBIC resonances, numerical simulations were performed on metasurfaces featuring translational asymmetry, OP asymmetry, and IP asymmetry. Here, the OP AMS and IP AMS are taken as representative examples. Figure 3a–c present the QBIC resonance reflection spectra under conditions of only broken translational symmetry, OP symmetry, and IP asymmetry, respectively. When g = 14 μm, the metasurface preserves translational symmetry; as g deviates from 14 μm, the translational symmetry is broken, thereby exciting high-Q SP-QBIC resonances. In Figure 3a, when only translational symmetry is broken, the QBIC resonance wavelength redshifts and the resonance linewidth broadens as g decreases. In Figure 3b,c, when only OP or IP symmetry is broken, the resonance wavelength undergoes a redshift or blueshift while the resonance linewidth gradually broadens as the degree of asymmetry increases. As shown in Figure 3a–c, compared with translationally asymmetric and OP asymmetric metasurfaces, the SP-QBIC resonance wavelength of the IP asymmetric metasurface varies most strongly with the asymmetry parameter. This can be explained by effective medium theory, breaking the IP symmetry of the metasurface induces a significant change in its effective refractive index, whereas breaking the translational symmetry and OP symmetry has a relatively minor effect on the effective refractive index. Consequently, the SP-QBIC resonance wavelength of the IP asymmetric metasurface undergoes a substantial shift. With the same asymmetry parameter, the OP asymmetric metasurface maintains a narrower linewidth, whereas both the translationally asymmetric and IP asymmetric metasurfaces exhibit relatively broad linewidths. This is primarily because IP asymmetry directly and efficiently modulates the radiative loss of the mode, leading to a more pro-

nounced change in linewidth. However, OP asymmetry affects the radiative loss more indirectly or gradually, resulting in a smaller linewidth variation and thus a narrower linewidth [20,33].

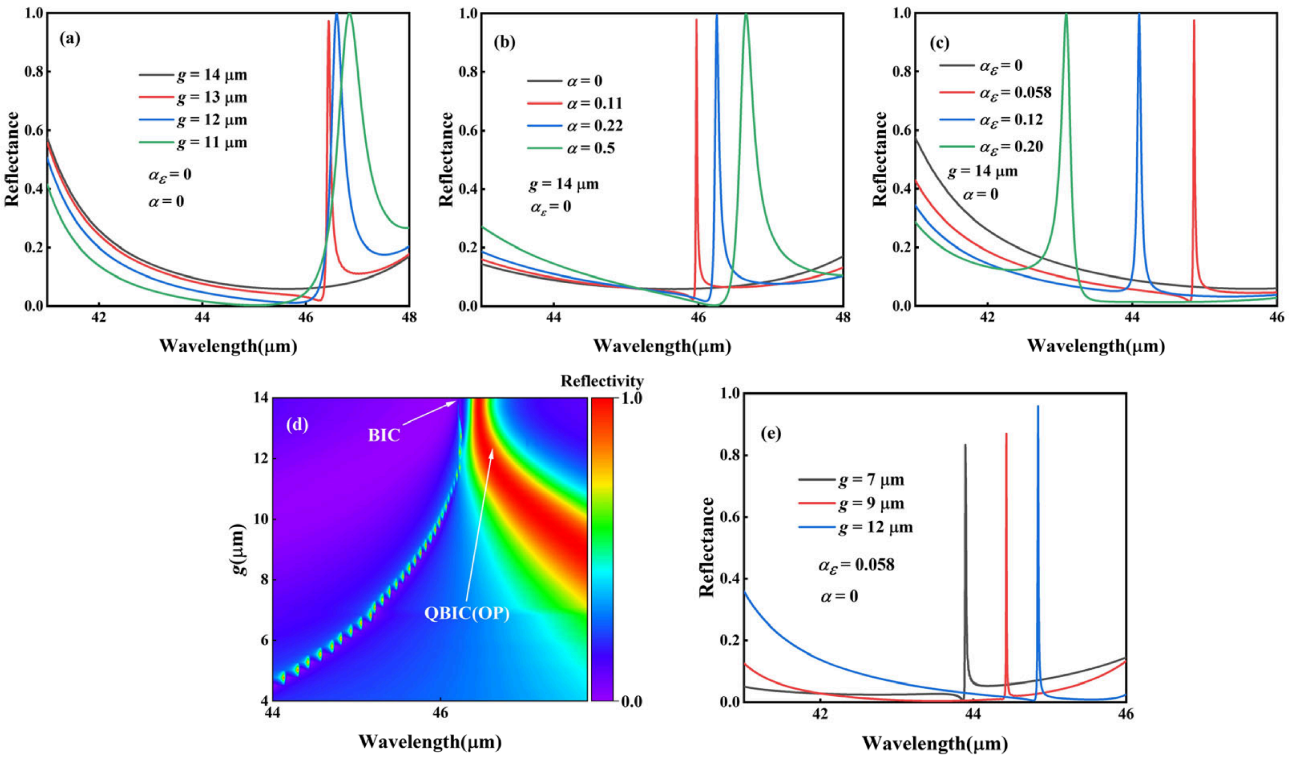


Figure 3. The effect of different asymmetry approaches on QBIC resonances. (**a**) Translational asymmetry; (**b**) out-of-plane asymmetry; (**c**) material asymmetry; (**d**) out-of-plane (α = 0.11); and translational asymmetry (**e**) material and translational asymmetry.

Figure 3d shows the resonance reflection spectra of the metasurface when both translational symmetry and OP symmetry are simultaneously broken. By comparing Figure 3a,b,d, when both OP and translational symmetry are broken, the metasurface not only excites a QBIC resonance solely governed by OP asymmetry, but also regenerates a new symmetry-protected QBIC resonance. As can be observed from Figure 3b,d, when both symmetries are simultaneously broken, decreasing the meta-atom gap spacing g causes the QBIC resonance wavelength determined by OP asymmetry to redshift, whereas the QBIC resonance wavelength determined jointly by OP and translational asymmetry exhibits a blueshift. Figure 3d further reveals that this new symmetry-protected BIC resonance generated by simultaneously breaking OP and translational symmetries possesses a narrower linewidth than resonances produced by breaking out-of-plane symmetry or translational symmetry alone. Analogously, simultaneously breaking IP and translational symmetry also yields a new symmetry-protected BIC resonance with a narrower linewidth, as shown in Figure 3e. The distinctive feature of the new BIC arising from the simultaneous breaking of two symmetries lies in the fact that it is not merely a simple superposition of two individual quasi-BICs. When both symmetry protections are broken, all protected modes become simultaneously unlocked [20]. Strong interactions among these distinct modes give rise to an entirely new coupled state with multiple symmetry-protected characteristics, which exhibits a narrower linewidth than modes arising from single-symmetry breaking [34,35].

3. Results and Discussion

To investigate the resonance characteristics of asymmetric metasurfaces, the SP-QBIC resonance reflection spectra of HOP and IP AMS under different asymmetry parameters were simulated and calculated, as shown in Figure 4. Figure 4b is a magnified inset of Figure 4a. Here, h_l = 2.7 μm, n_l = 2 (the corresponding dielectric material is HfO_2), g = 4.8 μm (broken translational symmetry), $\Phi = 90°$. As can be seen from the figure, although the SP-QBIC resonance wavelengths of HOP_u, HOP_b, and IP AMS all shift with increasing asymmetry parameters, the wavelength shift range of HOP AMS is significantly smaller than that of IP AMS. It can also be observed from Figure 4 that as the asymmetry parameter increases, the SP-QBIC resonance wavelength of HOP AMS gradually redshifts, while that of IP AMS gradually blueshifts. This is mainly because as the asymmetry parameter α_ε increases, the effective refractive index of IP AMS decreases, leading to a blueshift of the resonance wavelength. To more directly understand the influence of asymmetry parameters on the SP-QBIC resonance wavelengths of HOP and IP AMS. Figure 5a presents the variation in resonance wavelengths for the three asymmetric metasurfaces (HOP_u, HOP_b, and IP) under different asymmetry parameters. As shown in Figure 5a, when the asymmetric parameter α_ε increases from 0 to 0.3, the SP-QBIC resonance wavelength of IP AMS shifts by nearly 2.5 μm. Within the same range of asymmetry parameter α variation, the SP-QBIC resonance wavelengths of HOP_u and HOP_b AMS shift by only 0.5 μm and 0.7 μm, respectively. It can also be observed that within the same variation range of asymmetric parameter α, the SP-QBIC resonance wavelength shift range of HOP_u AMS is slightly smaller than that of HOP_b AMS.

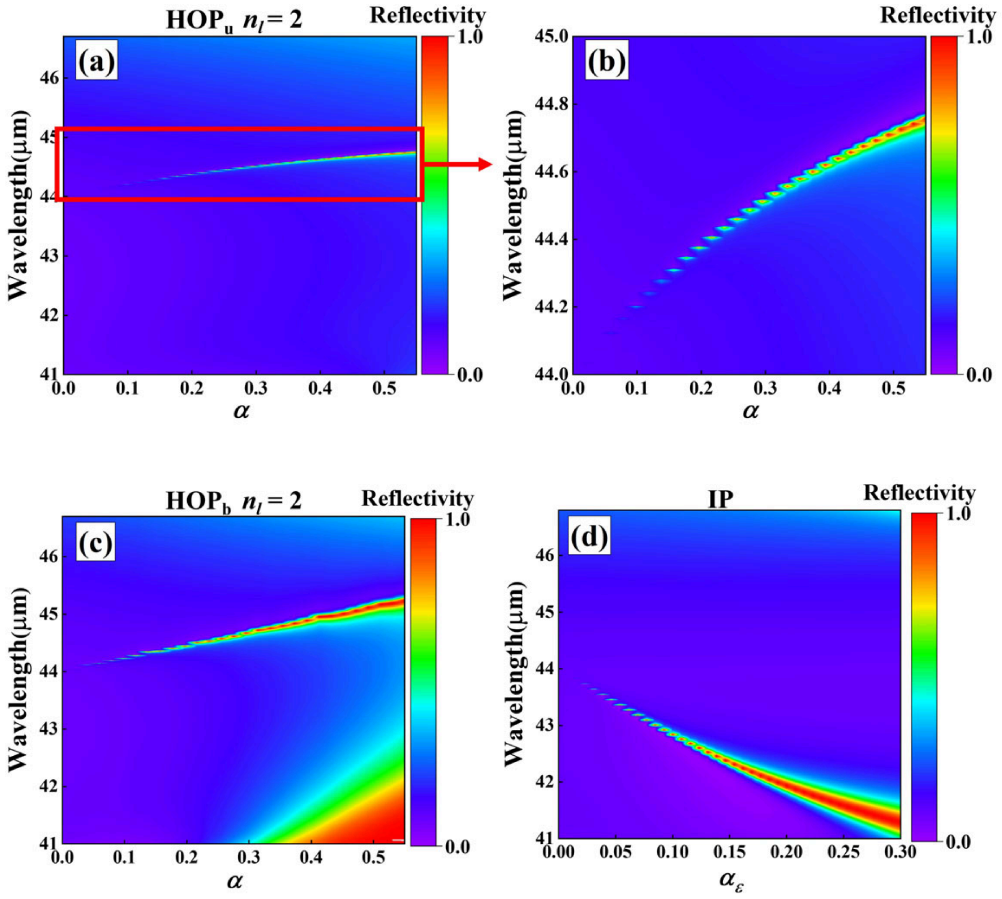


Figure 4. The effect of asymmetry parameters on metasurface reflection spectra. (**a**) HOP_u AMS; (**b**) magnified inset of Figure (**a**); (**c**) HOP_b AMS; (**d**) IP AMS.

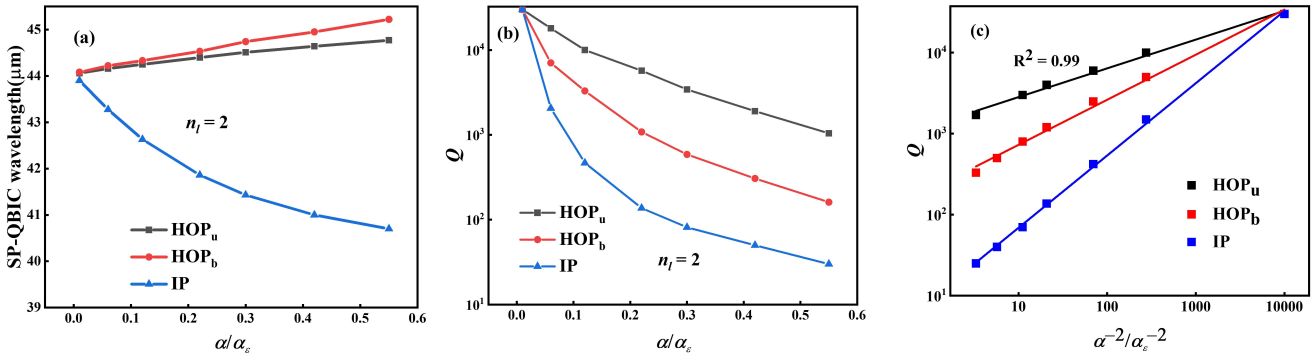


Figure 5. Effect of $\alpha/\alpha_\varepsilon$ on SP-QBIC resonance. (**a**) Effect of $\alpha/\alpha_\varepsilon$ on SP-QBIC resonance wavelength; (**b**) effect of $\alpha/\alpha_\varepsilon$ on SP-QBIC resonance Q factor; (**c**) relationship between Q factor and $\alpha^{-2}/\alpha_\varepsilon{}^{-2}$.

In addition to the QBIC resonance wavelength, Figure 4 shows that the SP-QBIC resonance linewidth of HOP AMS is also significantly narrower than that of IP AMS. Additionally, the SP-QBIC resonance linewidth of HOP_u AMS is also obviously narrower than that of HOP_b AMS. The above results indicate that the SP-QBIC resonance wavelength and Q factor of HOP AMS (the narrower the linewidth, the larger the Q factor) have stronger robustness against variations in asymmetry parameters, and the effect is better when the hetero material is located up the meta-atoms. To more intuitively understand the effect of asymmetry parameters on the Q factor of HOP_u, HOP_b, and IP AMS. The Q factor of the three asymmetric metasurfaces under different asymmetric parameters were calculated respectively. Figure 5b shows the Q factor of HOP_u, HOP_b, and IP AMS under different asymmetry parameters. It can be found that when the asymmetric parameter is small, the Q factors of three asymmetric metasurfaces maintain high values (above 10^4). As the asymmetry parameter increases, the Q factor of HOP_u AMS shows extremely strong robustness. For IP AMS, its Q factor decreases rapidly with increasing asymmetric parameter. Although the Q factor of HOP_b AMS also decreases with changes in asymmetry parameters, its robustness is clearly superior to that of IP AMS. Compared with Refs. [23–26], HOP_u AMS offers the distinct advantage of simultaneously enhancing the robustness of both the resonance wavelength and the Q factor. Figure 5c shows the relationship between Q factor and $\alpha_\varepsilon{}^{-2}/\alpha^{-2}$ (log-log scale), which exhibits a basically linear dependence. Fitting coefficient $R^2 = 0.99$. The evolution of the Q factor with $\alpha/\alpha_\varepsilon$ follows the universal behavior of BIC modes, showing the expected inverse quadratic trend ($Q \propto \alpha^{-2}$).

Figure 6 presents the magnetic field distributions at the resonance wavelength for the HOP_u, HOP_b, and IP AMS, where $\alpha/\alpha_\varepsilon = 0.11$. In the figure, black arrows represent the magnetic field vectors, while white arrows indicate the magnetic dipoles (MDs). A comparison of Figure 6a–c reveals that the three asymmetric metasurfaces exhibit essentially identical magnetic field distributions and magnetic field vectors, differing only in the magnetic energy intensity. Due to the higher Q factor of the HOP_u asymmetric metasurface, the localized magnetic energy is correspondingly stronger under the same excitation conditions. Additionally, two oppositely oriented MDs can be observed within each unit cell of all three asymmetric metasurfaces. These results demonstrate that the physical mechanisms underlying SP-QBIC resonance excitation in the three different asymmetric metasurfaces are similar, and that their distinction lies solely in the specific manner in which the metasurface symmetry is broken.

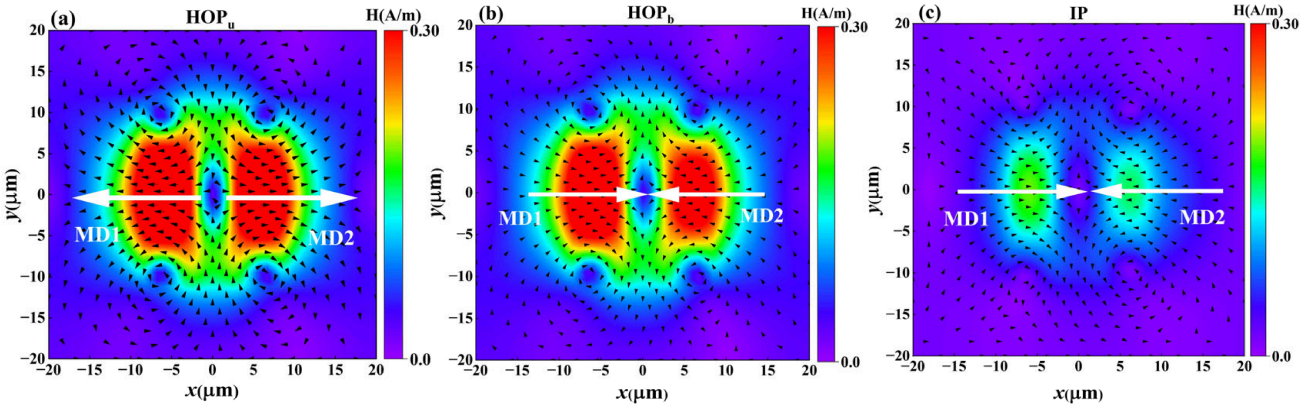


Figure 6. Magnetic field distributions of three asymmetric metasurfaces. (**a**) HOP_u AMS; (**b**) HOP_b AMS; (**c**) IP AMS.

To explore the *Q* factor of HOP AMS have strong robustness physical mechanism. The electric field distributions at the resonance wavelength of HOP AMS with different hetero-material thicknesses were calculated (*x*-*z* plane, $y = 0$ μm), as shown in Figure 7. Here, $n_l = 2$, $g = 4.8$ μm, $\Phi = 90°$. Figure 7a,c show the electric field distributions at the resonance wavelength for HOP_u and HOP_b AMS, respectively, here $h_l = 1.5$ μm ($\alpha = 0.16$). Figure 7b,d show the electric field distributions at the resonance wavelength for HOP_u and HOP_b AMS, respectively, here $h_l = 4.5$ μm ($\alpha = 0.5$). In the figures, the black line frames represent Si rectangular microstructures, and the white line frames represent hetero-material rectangular microstructures. O1 and O2 are the points of highest electric field intensity in the two rectangular microstructures, respectively. Δl_{O1} and Δl_{O2} represent the heights of the highest electric field intensity points O1 and O2 in the z-axis direction, respectively. Δl is used to represent the out-of-plane asymmetry degree of HOP AMS, where $\Delta l = |\Delta l_{O2} - \Delta l_{O1}|/(\Delta l_{O2} + \Delta l_{O1})$. $\Delta E = |E_1 - E2|/(E1 + E2)$ represents the in-plane asymmetry degree of HOP AMS, where $E1$ and $E2$ represent the total electric field intensities on the left and right sides of the metasurface unit at $x = 0$ μm, respectively. First, the electric field distribution of the metasurface unit cell is calculated and the corresponding data are exported. Then, the electric field intensity values at all points on the left (E1) and right (E2) sides of x = 0 μm are summed separately to obtain the total electric field intensity on each side of x = 0 μm. The total asymmetry degree of HOP AMS can be measured by $\Delta l + \Delta E$. As can be seen from Figure 7, both HOP_b AMS and HOP_u AMS exhibit varying degrees of OP and IP asymmetry between the two rectangular nanorods under different h_l. Comparing Figure 7a–d, it can be found that under the same h_l, the asymmetry degree ($\Delta l + \Delta E$) of HOP_u is smaller than that of HOP_b AMS. This indicates that under the same h_l, the asymmetry degree of HOP_u AMS is lower than that of HOP_b AMS, so HOP_u AMS has a higher *Q* factor under the same conditions, which agrees with Figure 5c. When $h_l = 1.5$ μm, the corresponding $\Delta l + \Delta E$ values for HOP_u and HOP_b AMS are 3.192% and 8.831%, respectively. When $h_l = 4.5$ μm, the corresponding $\Delta l + \Delta E$ values for HOP_u and HOP_b AMS are 9.595% and 29.99%, respectively. In Figure 7a–d, as h_l increases, the asymmetry degree ($\Delta l + \Delta E$) of both HOP_u and HOP_b AMS gradually increases. The increase of $\Delta l + \Delta E$ means the asymmetry degree of HOP_u and HOP_b AMS increases. Therefore, as h_l increases, the *Q* factors of HOP_u and HOP_b AMS gradually decrease, which reasonably explains the variation trend of *Q* factors for different metasurfaces with h_l in Figure 5c.

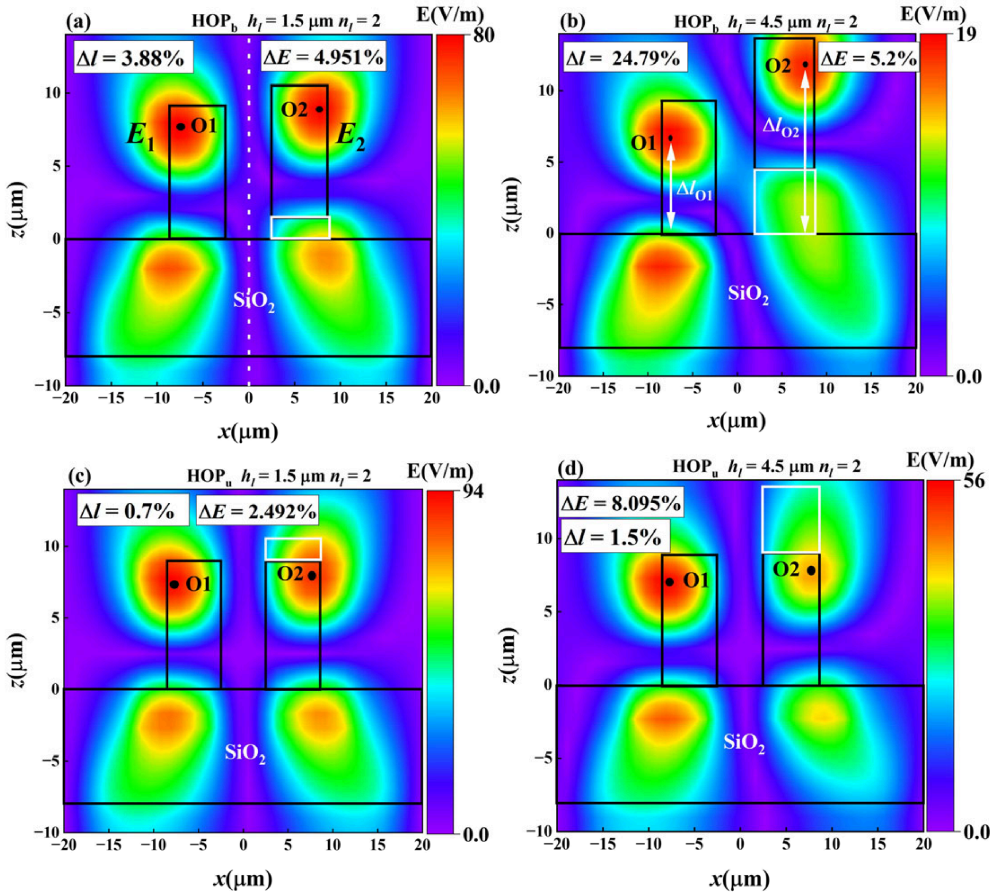


Figure 7. Electric field distributions (x-z plane) of HOP$_u$ and HOP$_b$ AMS at resonance wavelengths under different h_l values. HOP$_b$ AMS: (**a**) h_l = 1.5 μm and (**b**) h_l = 4.5 μm; HOP$_u$ AMS: (**c**) h_l = 1.5 μm and (**d**) h_l = 4.5 μm.

In addition to the thickness h_l of the hetero-material rectangular nanorods affecting the resonance of HOP$_u$ and HOP$_b$ AMS, the refractive index n_l of hetero-material also significantly influences their SP-QBIC resonance, as shown in Figure 8. Figure 8a,b respectively show the effect of n_l on the resonance spectra of HOP$_b$ and HOP$_u$ AMS. It can be observed that as n_l increases, the SP-QBIC resonance wavelengths of both AMS exhibit redshift, and the resonance reflectivity of HOP$_u$ AMS is lower when n_l is small. To more intuitively understand the effect of n_l on the resonance wavelengths of the two AMS. Figure 8c presents the corresponding SP-QBIC resonance wavelengths with different n_l. As can be seen from Figure 8c, the resonance wavelengths of both metasurfaces increase essentially linearly with n_l. It can also be observed from Figure 8a,b that as n_l increases, the resonance wavelength of HOP$_u$ AMS not only redshifts but its resonance linewidth also gradually broadens, whereas the resonance linewidth of HOP$_b$ AMS only narrows slightly. Since the resonance linewidth is directly related to the resonance Q factor, we calculated the Q factors of the resonances of the two metasurfaces with different n_l, as shown in Figure 8d. As the n_l increases, the SP-QBIC resonance Q factor of HOP$_u$ AMS decreases from 7×10^3 to 1×10^3. Unlike HOP$_u$ AMS, the SP-QBIC resonance Q factor of HOP$_b$ AMS shows only a slight increase with increasing n_l, with its Q factor varying around 1×10^3. From the above results, it can be concluded that the SP-QBIC resonance of HOP AMS can be tuned not only through its asymmetric parameter α, but also by tuning n_l. In particular, the resonance reflectivity, linewidth, and resonance wavelength of HOP$_u$ AMS can all be modulated through α and n_l, and the desired resonance spectra can be coordinated between α and n_l.

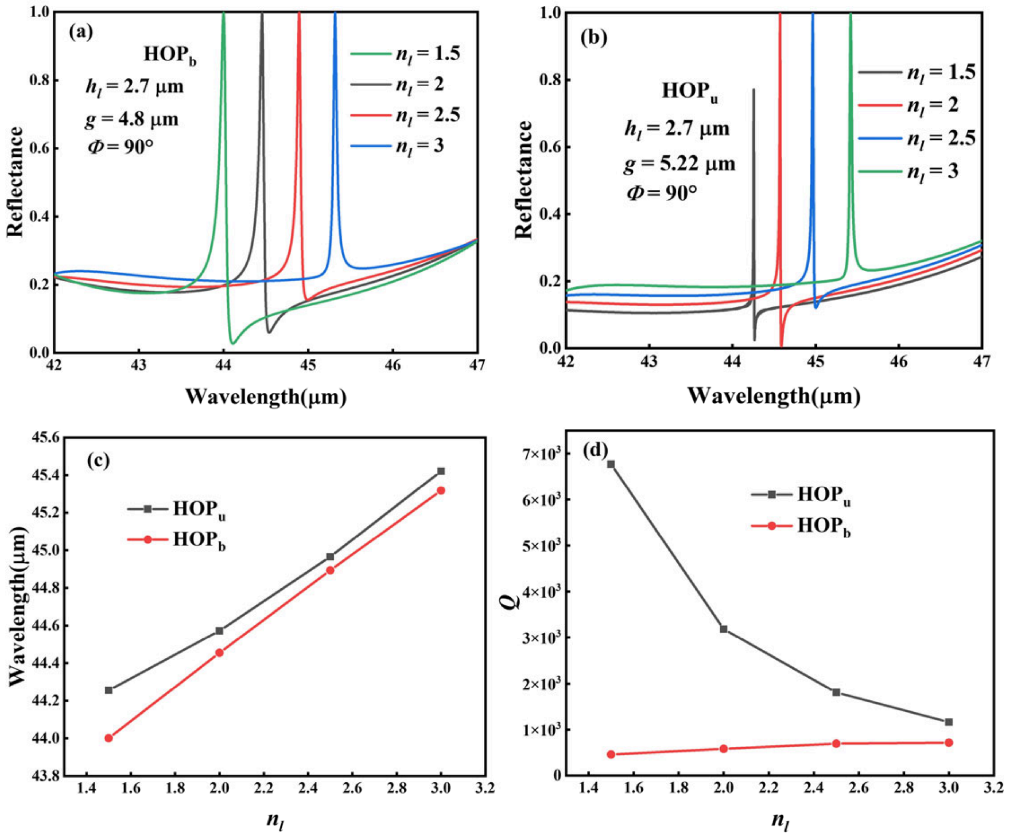


Figure 8. The effect of n_l on SP-QBIC resonance of HOP AMS. (**a**) The effect of n_l on SP-QBIC resonance of HOP$_b$ AMS; (**b**) the effect of n_l on SP-QBIC resonance of HOP$_u$ AMS; (**c**) the effect of n_l on SP-QBIC resonance wavelength of HOP AMS; (**d**) the effect of n_l on SP-QBIC resonance Q factor of HOP AMS.

To explore the mechanism of n_l effect on the Q factor of HOP AMS. The electric field distributions of HOP$_u$ and HOP$_b$ AMS under different n_l values (x-z plane, y = 0 μm) were calculated, as shown in Figure 9. At this moment, h_l = 2.7 μm (α = 0.3), g = 4.8 μm, Φ = 90°. Figure 9a,c show the electric field distribution of HOP$_u$ and HOP$_b$ AMS when n_l = 1.5, respectively. The Δl + ΔE for HOP$_b$ AMS is significantly higher (19.14%) than HOP$_u$ AMS (2.492%). This indicates that when n_l = 1.5, the asymmetry degree of HOP$_u$ AMS is significantly lower than that of HOP$_b$ AMS, resulting in a much higher Q factor for HOP$_u$ AMS than for HOP$_b$ AMS. When n_l increases from 1.5 to 3, the Δl + ΔE of HOP$_u$ AMS rises from 2.492% to 18.46%, while HOP$_b$ AMS's Δl + ΔE decreases from 22.14% to 21.08%. This suggests that as n_l increases from 1.5 to 3, the Q factor of HOP$_u$ AMS gradually declines, while that of HOP$_b$ AMS increases to some extent, which aligns well with the results in Figure 8d.

During the fabrication of micro/nanoscale devices, fabrication errors are inevitable and lead to deviations between the actual metasurface devices and theoretical designs. Therefore, investigating the impact of fabrication errors on metasurface performance is critically important. Figure 10 shows the influence of fabrication errors in the meta-atom width (w) and length (L) on the QBIC resonances of the HOP$_u$ and HOPb asymmetric metasurfaces. Figure 10a,b present the QBIC resonance spectra of the two asymmetric metasurfaces when w varies within a ±5% fabrication tolerance. As can be seen from these figures, the resonance spectra redshift and the resonance linewidth become narrower as w increases. Figure 10c directly displays the QBIC resonance wavelength and Q factor of the two asymmetric metasurfaces at different values of w. It can be observed that within the ±5% fabrication error range of w, the resonance wavelength of both asymmetric

metasurfaces shifts by only 0.5 μm, while the *Q* factor also exhibits strong robustness. Similar to the effect of w fabrication errors, the QBIC resonance shifts when *L* varies within a ±5% fabrication tolerance, whereas the resonance linewidth remains essentially unchanged, as detailed in Figure 10d,e. Figure 10f directly illustrates the influence of *L* on the QBIC resonance wavelength and *Q* factor. As can be seen, both the resonance wavelength and *Q* factor of the two asymmetric metasurfaces remain essentially stable within the ±5% fabrication error range of *L*, with the maximum shift in resonance wavelength being only 0.5 μm.

To verify the HOP AMS as illustrated in Figure 1 can excite polarization wavelength stable SP-QBIC resonance. The SP-QBIC resonance reflection spectra of HOP_u and HOP_b AMS at different polarization angles were calculated. The specific results are shown in Figure 11. From Figure 11a,b, when g = 5.22 μm or g = 4.8 μm, HOP_u or HOP_b AMS exhibit polarization wavelength stable characteristics. At this point, h_l = 2.7 μm and n_l = 2. As the polarization angle gradually increases from 0° to 90°, the QBIC resonance wavelengths of both HOP_u and HOP_b AMS remain basically stable. However, the resonance linewidth of HOP_u AMS is significantly narrower than that of HOP_b AMS. It can be seen from Figure 4, where under the same conditions, the SP-QBIC resonance linewidth of HOP_u AMS is much narrower than that of HOP_b AMS.

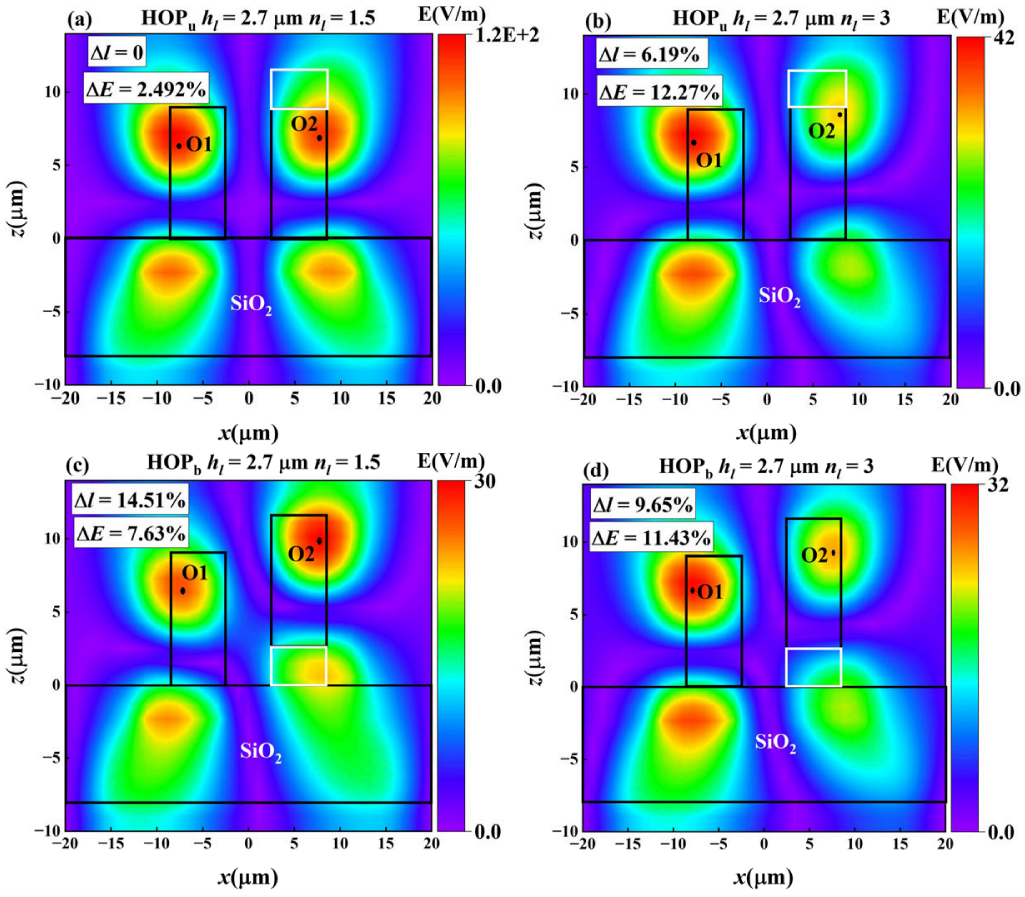


Figure 9. Electric field distribution (*x*-*z* plane) of HOP_u AMS at resonance wavelength for different n_l: (**a**) n_l = 1.5 and (**b**) n_l = 3; electric field distribution (*x*-*z* plane) of HOP_b AMS at resonance wavelength for different n_l. (**c**) n_l = 1.5 and (**d**) n_l = 3.

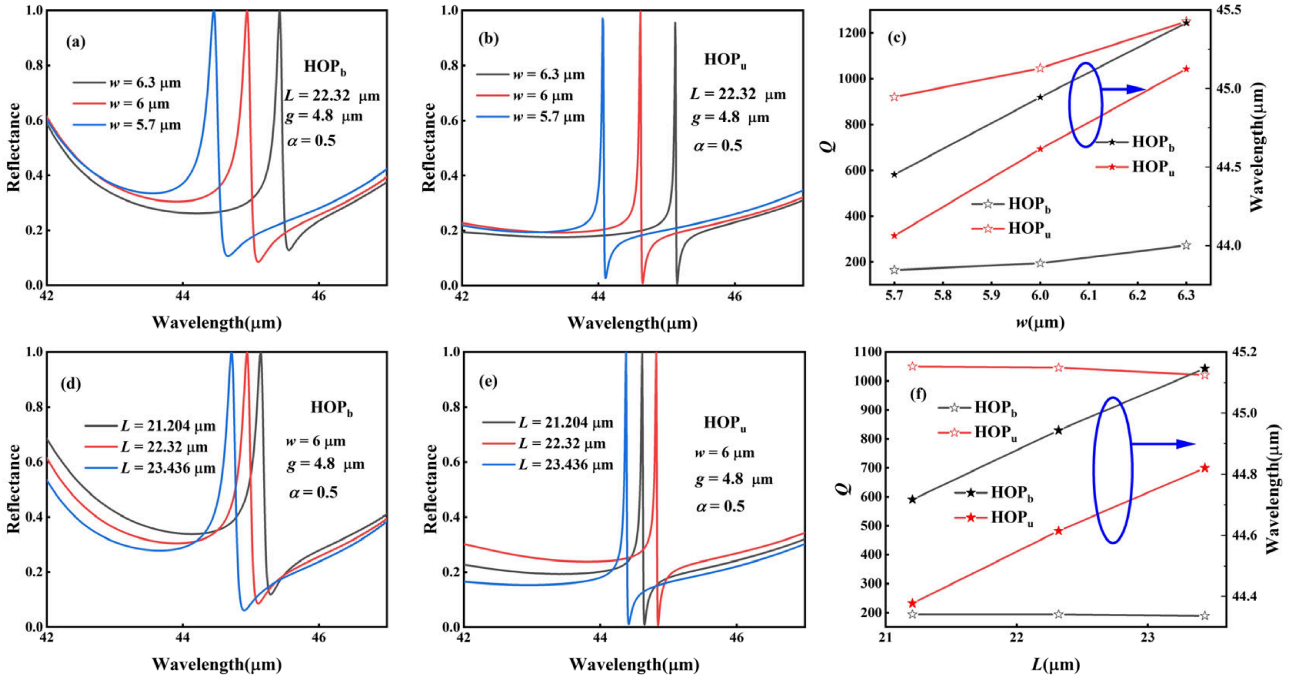


Figure 10. Effect of fabrication errors on resonances. The influence of meta-atom width w on QBIC resonances in the (**a**) HOP_b AMS and (**b**) HOP_u AMS. (**c**) QBIC resonance wavelength and Q factor as a function of w. The influence of meta-atom length L on QBIC resonances in the (**d**) HOP_b AMS and (**e**) HOP_u AMS. (**f**) QBIC resonance wavelength and Q factor as a function of L.

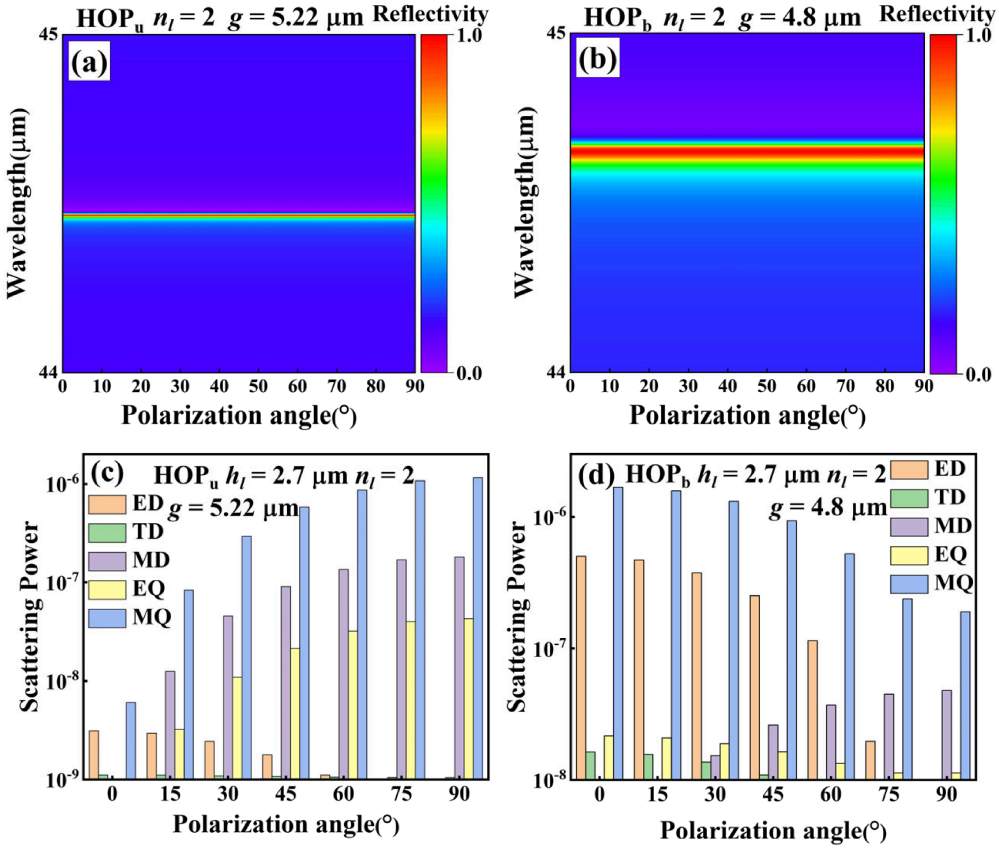


Figure 11. Reflectance spectra and multipole decomposition. (**a**,**b**) Reflectance spectra of HOP_u AMS and HOP_b AMS at different polarization angles; (**c**,**d**) multipole scattering power of HOP_u AMS and HOP_b AMS at different polarization angles.

To explore the physical properties that enable polarization wavelength stable in HOP AMS. Multipole decomposition was carried out, and the multipole scattering power at different polarization angles was calculated, as shown in Figure 11c,d. In this study, only the scattering powers of five multipoles were calculated: electric dipole (ED), electric quadrupole (EQ), MD, magnetic quadrupole (MQ), and toroidal dipole (TD). This is because higher-order multipoles have relatively small scattering powers and make minor contributions to the excitation of SP-QBIC resonance. For HOP_u AMS and HOP_b AMS, with varying polarization angles, their respective multipole scattering powers display significant changes. The main reason that both asymmetric metasurfaces can excite SP-QBIC resonance is MQ. For HOP_u AMS, the scattering power of MQ increases with the polarization angle, whereas for HOP_b AMS, the MQ scattering power gradually decreases as the polarization angle increases. In addition, as the polarization angle Φ increases, the ED scattering power of the two asymmetric metasurfaces decreases, but the MD scattering power increases. When $\Phi = 0$, the SP-QBIC resonance in HOP_u AMS is formed not only because of MQ but is also affected by ED. However, when $\Phi \neq 0$, the contributions of MD and EQ to the excitation of SP-QBIC resonance in HOP_u AMS gradually increase, and the contribution of ED becomes negligible. For HOP_b AMS, within $\Phi < 60°$, the contribution of ED to the excitation of SP-QBIC resonance cannot be neglected, but when $\Phi > 60°$, the contribution of ED gradually weakens while the contribution of MD gradually increases.

To further explore the physical mechanism that HOP AMS can excite polarization wavelength stable SP-QBIC resonance, the electromagnetic field distributions of HOP AMS at polarization angles $\Phi = 0°$, $30°$, $60°$ and $90°$ were calculated, as shown in Figures 12 and 13. Figure 12 shows the electric field distributions of the HOP_u and HOP_b AMS at different polarization angles. Figure 12a–d present the electric field distributions of the HOP_u AMS, while Figure 12e–h show those of the HOP_b AMS. It can be seen from Figure 12 that the HOP_u and HOP_b asymmetric metasurfaces exhibit essentially identical electric field distributions at the same polarization angle, differing only in electric field intensity. Furthermore, the figure reveals that the electric field distributions of the HOP AMS at $\Phi = 0°$ and $30°$ are completely different from those at $\Phi = 60°$ and $90°$. This indicates that the underlying physical mechanisms enabling the HOP AMS to maintain polarization wavelength stable performance at $\Phi = 0°$ and $30°$ differ from those at $\Phi = 60°$ and $90°$.

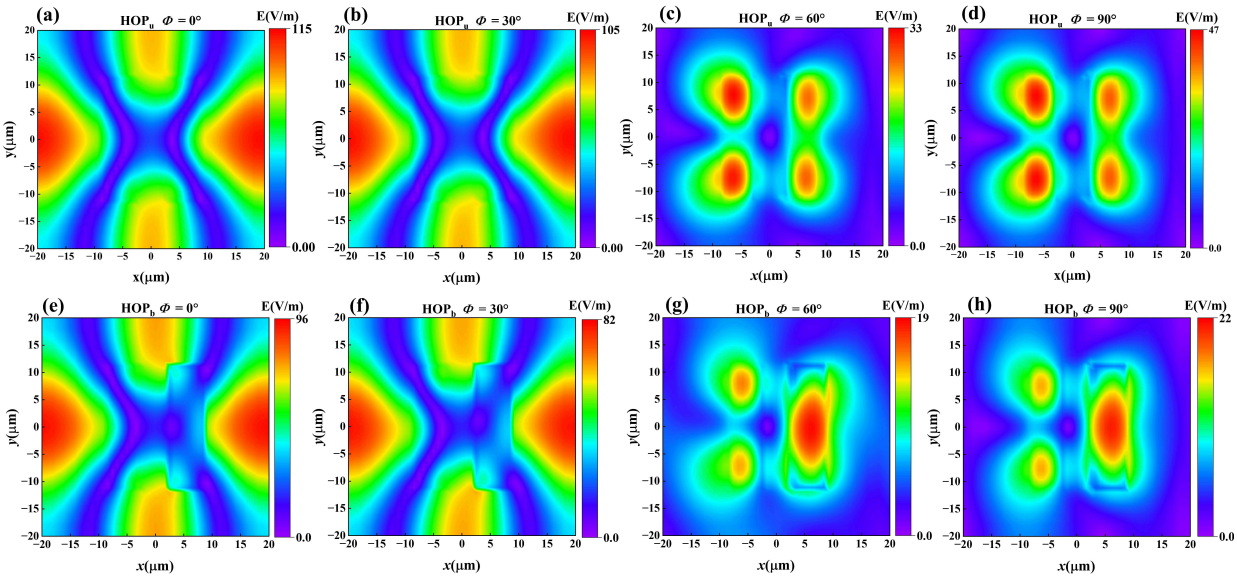


Figure 12. Electric field distribution of HOP AMS at different polarization angles. (**a**–**d**) HOP_u AMS; (**e**–**h**) HOP_b AMS.

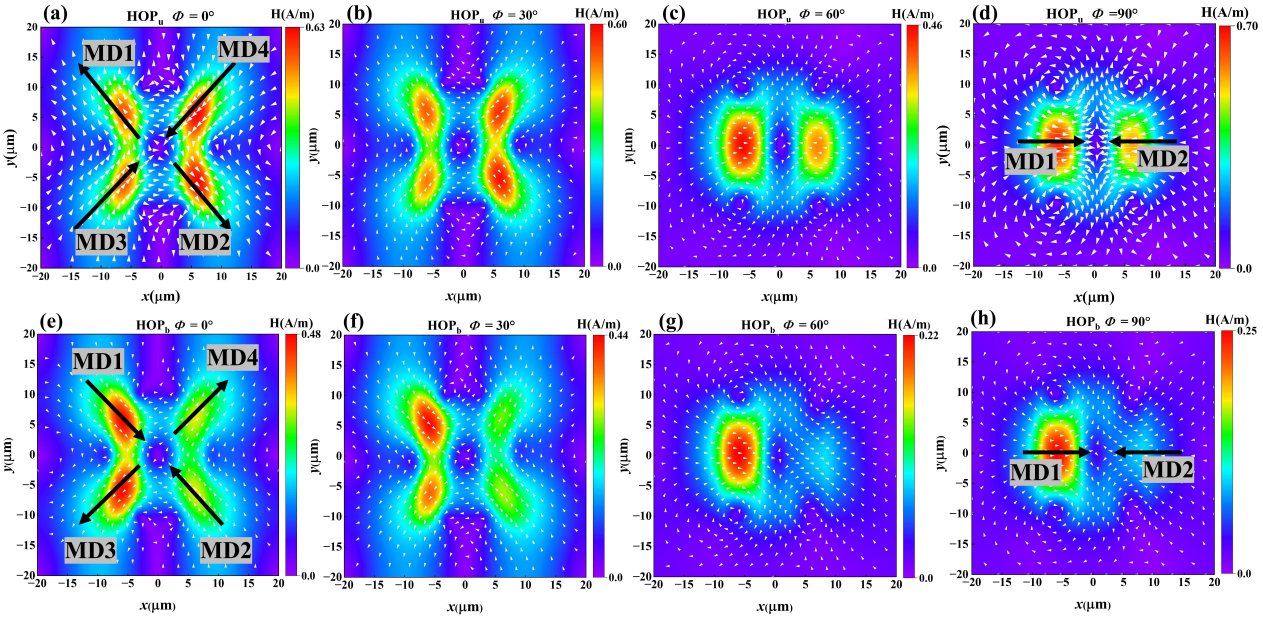


Figure 13. Magnetic field distribution of HOP AMS at different polarization angles. (**a**–**d**) HOP_u AMS; (**e**–**h**) HOP_b AMS.

The magnetic field distributions of the HOP AMS in Figure 13 further corroborate this conclusion. Figure 13 shows the magnetic field distributions of the HOP_u and HOP_b AMS at different polarization angles. In the figure, white arrows represent the magnetic field vectors and black arrows indicate the MDs. Figure 13a–d present the magnetic field distributions of the HOP_u AMS, while Figure 13e–h show those of the HOP_b AMS. Consistent with the electric field distributions, the magnetic field distributions of the HOP_u and HOP_b asymmetric metasurfaces are essentially identical at the same polarization angle. From Figure 13a,b,e,f, it can be observed that at $\Phi = 0°$ and 30°, the HOP_u and HOP_b asymmetric metasurfaces form four MDs with different orientations within a single metasurface unit cell, thereby constituting an MQ. However, as can be seen from Figure 13c,d,g,h, at $\Phi = 60°$ and 90°, the HOP_u and HOP_b asymmetric metasurfaces can only form two MDs with different orientations within a single unit cell; consequently, the MQ can only be formed through coupling with adjacent metasurface unit cells. A combined analysis of Figures 11–13 reveals that although the polarization wavelength stable SP-QBIC resonances in the HOP AMS at different polarization angles all originate from MQs, the formation mechanisms of the MQ differ across polarization angles. This demonstrates that the physical mechanisms enabling the HOP AMS to achieve polarization wavelength stable SP-QBIC resonances are not completely identical across different polarization angles.

As shown in Figure 11, in order for HOP_u and HOP_b AMS to achieve polarization wavelength stable, n_l, h_l and g are the key parameters. When n_l and h_l change, g must be adjusted so that HOP_u AMS and HOP_b AMS can excite polarization wavelength stable SP-QBIC resonance. Therefore, we calculated the values of g required for HOP AMS to excite polarization wavelength stable SP-QBIC resonance under different n_l and h_l, as specifically illustrated in Figure 14. As shown in Figure 14a, when n_l ($n_l = 2$) is fixed, g must gradually decrease with the increase in h_l in order for both types of HOP AMS to maintain polarization wavelength stable. However, the g value corresponding to HOP_u AMS is significantly greater than that of HOP_b AMS. Figure 14b shows the values of g required for HOP AMS to maintain polarization wavelength stable at different n_l values when $h_l = 2.7$ μm. As n_l increases, the g required for HOP AMS to excite polarization wavelength stable SP-QBIC resonance gradually decreases.

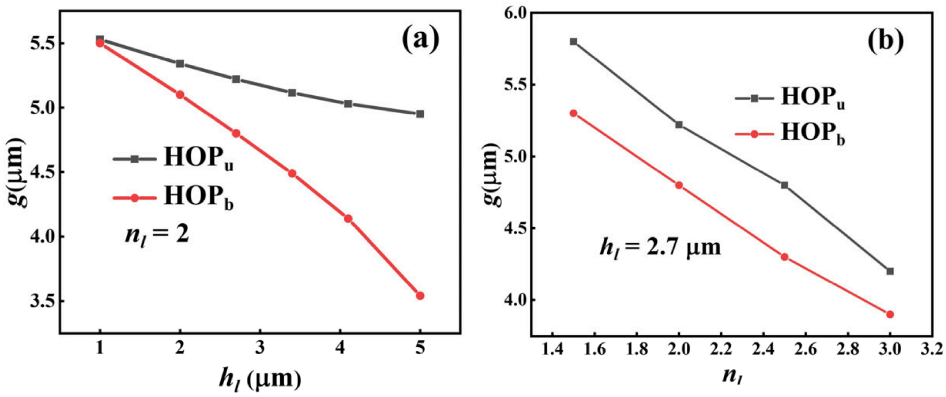


Figure 14. The g corresponding to polarization-independent conditions of HOP AMS. (**a**) When n_l is fixed, the HOP asymmetric metasurface achieves the polarization-independent relationship between h_l and g; (**b**) when h_l is fixed, the HOP asymmetric metasurface achieves the polarization-independent relationship between n_l and g.

Subsequently, the effect of g on polarization-wavelength stability was investigated by numerically calculating the resonance wavelength difference between $\Phi = 0°$ and 90° for various values of g, as shown in Figure 15. It can be seen from Figure 15a,b that the absolute value of the polarization wavelength difference is highly robust against variations in g. Although the polarization wavelength stability of the HOP$_b$ (HOP$_u$) AMS is broken once g deviates from 4.8 μm (5.22 μm), causing the polarization wavelength difference to gradually increase, the maximum difference remains only 0.3 μm even when g deviates by 8% from its original value. Figure 15c presents the reflection spectra of the HOP$_u$ AMS under different polarization conditions at g = 5.02 μm. As the figure shows, once g deviates from the polarization wavelength stable spacing, the SP-QBIC resonance in the HOP$_u$ AMS loses its polarization wavelength stability. Consequently, the resonance wavelengths differ under different polarization conditions. However, even at g = 5.02 μm (approximately 4% deviation from the original value), the polarization wavelength difference is only 0.1 μm, exhibiting considerable robustness.

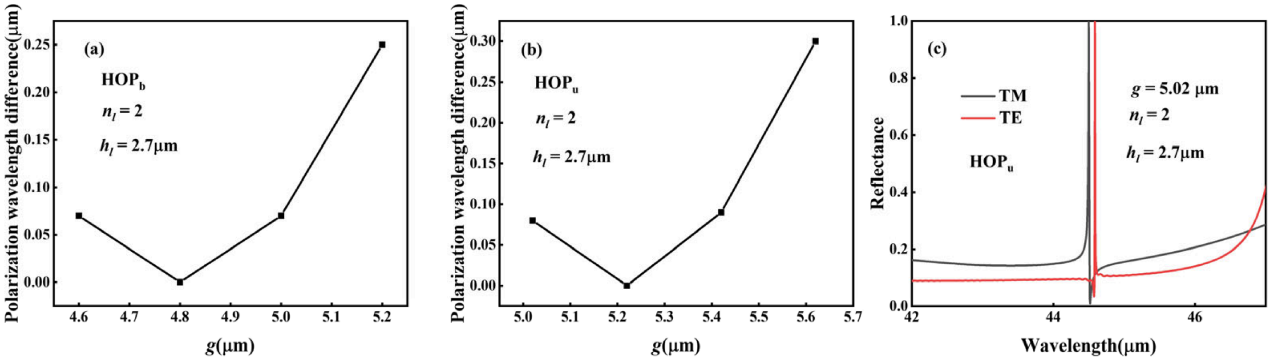


Figure 15. The effect of meta-atom spacing g on polarization wavelength stable. (**a**) HOP$_b$ AMS; (**b**) HOP$_u$ AMS; (**c**) resonant reflection spectra of HOP$_u$ AMS under different polarizations.

Table 1 presents a comparison of existing studies on achieving SP-QBIC resonance robustness enhancement and polarization wavelength stabilization using non-rotationally symmetric metasurfaces. Through this comparison, it can be observed that current research has at most achieved stabilization of the SP-QBIC resonance wavelength and the Q factor, but cannot simultaneously stabilize the SP-QBIC resonance wavelength, Q factor, and polarization wavelength. This study unifies these three aspects; utilizing the non-

rotationally symmetric metasurface proposed herein, simultaneous stabilization of the SP-QBIC resonance wavelength, Q factor, and polarization wavelength is achieved.

Table 1. Studies on robust enhancement of SP-QBIC resonances and polarization-wavelength stability based on non-rotationally symmetric metasurfaces.

Year [Ref]	Q Stable	Wavelength Stable	Polarization Wavelength Stable
2023 [29]	Yes	Yes	No (experiment)
2023 [36]	No	No	Yes (simulation)
2025 [3]	No	Yes	No (experiment)
This work	Yes	Yes	Yes (simulation)

4. Conclusions

A hetero-material out-of-plane metasurface has been proposed, based on which not only can polarization wavelength stable SP-QBIC resonances be excited, but the robustness of SP-QBIC resonances to asymmetric parameter variations is significantly enhanced. The effects of the asymmetric parameter α on the HOP_u and HOP_b AMS resonance spectra were simulated. It can be found that both HOP AMS types not only possess stable SP-QBIC resonance wavelengths but also exhibit strong robustness of SP-QBIC resonance Q factors against variations in α. Notably, HOP_u AMS exhibits superior performance. The stability of the wavelength in HOP AMS as α varies is attributed to the electric field being localized within the Si meta- atoms, resulting in minimal disturbance to the electric field distribution of the metasurface when α changes. Furthermore, the stronger robustness of the resonance Q value in HOP_u AMS arises from the fact that the asymmetry degree in HOP_u AMS changes significantly less than that in HOP_b AMS as α increases. In addition to the asymmetric parameter, the refractive index n_l of the hetero-material also significantly affects the SP-QBIC resonance wavelength and Q value of HOP AMS. As n_l increases, the SP-QBIC resonance wavelengths of both HOP_u AMS and HOP_b AMS exhibit a redshift, and the Q value of HOP_u AMS rapidly decreases with an increase in n_l This is mainly because the asymmetry degree in HOP_u AMS significantly increases as n_l. increases. Finally, simulations of the SP-QBIC resonance reflection spectra of HOP AMS at different incident light polarization angles were conducted, revealing that under specific structural parameters, the HOP AMS can excite polarization wavelength stable SP-QBIC resonances. The physical mechanisms by which HOP_u AMS and HOP_b AMS can excite polarization wavelength stable SP-QBIC resonances were explored. The HOP_u AMS proposed in this study can be applied in areas such as laser and highly sensitive biochemical sensors.

Author Contributions: Conceptualization, Z.G. and Z.C.; methodology, Z.G.; software, Z.G. and Z.Y.; validation, J.X., and Z.G.; formal analysis, Z.G.; investigation, Z.G.; resources, Z.C.; data curation, Z.G.; writing—original draft preparation, Z.G.; writing—review and editing, J.X.; visualization, Z.Y.; supervision, Z.C.; project administration, J.X.; funding acquisition, Z.G. All authors have read and agreed to the published version of the manuscript.

Funding: This research was funded by the Zhejiang Provincial Natural Science Foundation of China (Grant No. LQ23F040001), the National Natural Science Foundation of China (Grant No. 61575008), Quzhou Science and Technology Plan Project (2024K194, 2025K229), 2024 Annual Domestic Visiting Scholars Teacher Professional Development Program (FX2024186).

Data Availability Statement: The data presented in this study are available from the corresponding author upon reasonable request.

Conflicts of Interest: The authors declare no conflict of interest.

References

1. Neumann, J.V.; Wigner, E.P. Über merkwürdige diskrete eigenwerte. *Phys. Z.* **1929**, *30*, 465–467.
2. Kang, M.; Liu, T.; Chan, C.T.; Xiao, M. Applications of bound states in the continuum in photonics. *Nat. Rev. Phys.* **2023**, *5*, 659–678. [CrossRef]
3. Watanabe, K.; Nagao, T.; Iwanaga, M. Low-contrast BIC metasurfaces with quality factors exceeding 100,000. *Nano Lett.* **2025**, *25*, 2777–2784. [CrossRef] [PubMed]
4. Zhang, J.; Feng, Z.; Sun, X. Realization of bound states in the continuum in anti-PT-symmetric optical systems: A proposal and analysis. *Laser Photonics Rev.* **2023**, *17*, 00079. [CrossRef]
5. Qin, M.; Wu, F.; Liu, T.; Zhang, D.; Xiao, S. Enhanced third-harmonic generation and degenerate four-wave mixing in an all-dielectric metasurface via Brillouin zone folding induced bound states in the continuum. *Phys. Rev. B* **2025**, *111*, 035414. [CrossRef]
6. Huang, L.; Xu, L.; Powell, D.A.; Padilla, W.J.; Miroshnichenko, A.E. Resonant leaky modes in all-dielectric metasystems: Fundamentals and applications. *Phys. Rep.* **2023**, *1008*, 1–66. [CrossRef]
7. Liu, T.; Qin, M.; Qiu, J.; Tu, X.; Qiu, H.; Wu, F.; Yu, T.; Liu, Q.; Xiao, S. Polarization-independent enhancement of third-harmonic generation empowered by doubly degenerate quasi-bound states in the continuum. *Nano Lett.* **2025**, *25*, 3646–3652. [CrossRef] [PubMed]
8. Chen, M.-H.; Lee, Y.-T.; Xing, D.; Abdullah, M.; Asri, R.I.M.; Kamal, A.S.A.; Lin, B.-W.; Wang, Z.; Delaunay, J.-J. Ultraviolet chiral lasing in in-plane photonic crystal via quasi-bound state in the continuum. *Nano Lett.* **2025**, *25*, 9809–9816. [CrossRef] [PubMed]
9. Zhao, D.; Zhang, L.; Zhu, W.; Zhou, Y. Low-threshold lasing action driven by chiral quasi-bound state in the continuum in planar metasurface. *J. Nanophotonics* **2025**, *19*, 036006. [CrossRef]
10. Jiang, X.W.; Fang, B.; Zhan, C.L. Enhancing the Goos-Hänchen shift based on quasi-bound states in the continuum through material asymmetric dielectric compound gratings. *Chin. Phys. B* **2024**, *33*, 034206. [CrossRef]
11. Ma, Z.; Shi, Y.; Chen, Y.; Xue, Y.; Wan, G.; Zhang, C.; Jing, H.; Kuang, L.-M.; Zhou, X. Inverse design of quasi-bound states in the continuum metasurface for the polarization independent enhancement of Goos-Hänchen shift. *Sci. China Phys. Mech.* **2024**, *67*, 124211. [CrossRef]
12. Tse, J.T.Y.; Enomoto, T.; Murai, S.; Tanaka, K. Modelling purcell enhancement of metasurfaces supporting quasi-bound states in the continuum. *Nanophotonics* **2025**, *14*, 5407–5415. [CrossRef] [PubMed]
13. Schiattarella, C.; Romano, S.; Sirleto, L.; Mocella, V.; Rendina, I.; Lanzio, V.; Riminucci, F.; Schwartzberg, A.; Cabrini, S.; Chen, J.; et al. Directive giant upconversion by supercritical bound states in the continuum. *Nature* **2024**, *626*, 765–771. [CrossRef] [PubMed]
14. Yang, F.; She, S.; Li, J.; Yue, Z.; Zhang, Q.; Zhang, Y.; Ding, X.; Yao, J. Terahertz biosensor supported by quasi-bound states in the continuum for lung cancer cell sensing. *Chin. Opt. Lett.* **2025**, *23*, 023604. [CrossRef]
15. Sang, T.; Mi, Q.; Yang, C.; Zhang, X.; Wang, Y.; Ren, Y.; Xu, T. Achieving asymmetry parameter-insensitive resonant modes through relative shift–induced quasi-bound states in the continuum. *Nanophotonics* **2024**, *13*, 1369–1377. [CrossRef] [PubMed]
16. Luo, X.; Zhang, F.; Pu, M.; Ha, Y.; Yu, S.; Bao, H.; He, Q.; Gao, P.; Guo, Y.; Xu, M.; et al. Breaking symmetry dependency of symmetry-protected bound states in the continuum via metasurfaces. *Chin. Opt. Lett.* **2025**, *23*, 053601. [CrossRef]
17. Chen, J.; Liu, J.; Shu, F.; Du, Y.; Hong, Z. Merging of accidental bound states in the continuum in symmetry and symmetry-broken terahertz photonic crystal slabs. *Nanomaterials* **2025**, *15*, 451. [CrossRef] [PubMed]
18. Yan, X.; Wang, X.; Lin, Q.; Wang, L.; Liu, G. Active Formation of Friedrich-Wintgen Bound States in the Continuum in a Hybrid Plasmonic-Photonic Structure. *Adv. Photon. Res.* **2025**, *6*, 00145. [CrossRef]
19. Wang, Y.; Liu, J.; Shu, F.; Du, Y.; Hong, Z. Dual Friedrich-Wintgen bound states in the continuum in asymmetric all-silicon photonic crystal slabs. *Opt. Laser Eng.* **2025**, *193*, 109105. [CrossRef]
20. Koshelev, K.; Lepeshov, S.; Liu, M.; Bogdanov, A.; Kivshar, Y. Asymmetric metasurfaces with high-Q resonances governed by bound states in the continuum. *Phys. Rev. Lett.* **2018**, *121*, 193903. [CrossRef] [PubMed]
21. Jin, R.; Huang, L.; Zhou, C.; Guo, J.; Fu, Z.; Chen, J.; Wang, J.; Li, X.; Yu, F.; Chen, J.; et al. Toroidal dipole BIC-driven highly robust perfect absorption with a graphene-loaded metasurface. *Nano Lett.* **2023**, *23*, 9105–9113. [CrossRef] [PubMed]
22. Hu, H.; Zhou, C.; Zhang, Y.; Hu, M.-X.; Peng, J.; Tang, H.; Huang, L.; Liu, J.; Guan, C.; Zhu, Z.; et al. Robust chirality via merging accidental BICs with net zero topological charge. *Elight* **2026**, *6*, 00126. [CrossRef]
23. You, S.; Zhou, M.; Xu, L.; Chen, D.; Fan, M.; Huang, J.; Ma, W.; Luo, S.; Rahmani, M.; Zhou, C.; et al. Quasi-bound states in the continuum with a stable resonance wavelength in dimer dielectric metasurfaces. *Nanophotonics* **2023**, *12*, 2051–2060. [CrossRef] [PubMed]
24. You, S.; He, H.; Zhang, Y.; Duan, H.; Wang, L.; Wang, Y.; Luo, S.; Zhou, C. Resonance wavelength stabilization of quasi-bound states in the continuum constructed by symmetry breaking and area compensation. *Nano Lett.* **2024**, *24*, 15300–15307. [CrossRef] [PubMed]

25. Liang, S.; Wang, W.; Huo, Y.; Yue, Q.; Cai, Y.; Ning, T. Ultralow level all-optical self-switching empowered by merging bound states in the continuum. *Appl. Phys. Lett.* **2025**, *127*, 071701. [CrossRef]
26. Huang, L.; Li, S.; Zhou, C.; Zhong, H.; You, S.; Li, L.; Cheng, Y.; Miroshnichenko, A.E. Realizing ultrahigh-Q resonances through harnessing symmetry-protected bound states in the continuum. *Adv. Funct. Mater.* **2024**, *34*, 202309982. [CrossRef]
27. Wu, Q.; Niu, L.-T.; Wu, S. Band-folding quasi-bound states in the continuum supported by dimer nanobars with symmetry broken along z-direction. *J. Nanophotonics* **2024**, *18*, 046011. [CrossRef]
28. Zhou, Y.; Ni, B.; Ni, H.; Zhou, X.; Yang, L.; Chang, J. Quasi-bound states in the continuum induced by in-plane and out-of-plane asymmetry in all-dielectric metasurfaces. *Jap. J. Appl. Phys.* **2024**, *63*, 090904. [CrossRef]
29. Wang, Z.; Sun, J.; Li, J.; Wang, L.; Li, Z.; Zheng, X.; Wen, L. Customizing 2.5D out-of-plane architectures for robust Plasmonic bound-states-in-the-continuum metasurfaces. *Adv. Sci.* **2023**, *10*, 202206236.
30. Sun, G.; Chao, X.; Liu, J.Q.; Yu, J.; Xu, G. Dual polarization-independent quasi-bound states in the continuum in a hetero-out-of-plane dielectric metasurface. *Opt. Lett.* **2024**, *49*, 7094–7097. [CrossRef] [PubMed]
31. Kühner, L.; Wendisch, F.J.; Antonov, A.A.; Bürger, J.; Hüttenhofer, L.; Menezes, L.d.S.; Maier, S.A.; Gorkunov, M.V.; Kivshar, Y.; Tittl, A. Unlocking the out-of-plane dimension for photonic bound states in the continuum to achieve maximum optical chirality. *Light-Sci. Appl.* **2023**, *12*, 250. [CrossRef] [PubMed]
32. Berté, R.; Weber, T.; de Souza Menezes, L.; Kühner, L.; Aigner, A.; Barkey, M.; Wendisch, F.J.; Kivshar, Y.; Tittl, A.; Maier, S.A. Permittivity-asymmetric quasi-bound states in the continuum. *Nano Lett.* **2023**, *23*, 2651–2658. [CrossRef] [PubMed]
33. Jiang, X.; Zhan, C.; Zhang, G.; He, X.; Xie, L. Symmetry-protected bound states in the continuum resonance with wavelength stable and Q factor strong robustness excited by hetero-out-of-plane metasurface. *Opt. Commun.* **2025**, *596*, 132464. [CrossRef]
34. Kim, K.H.; Cho, M.C. Extremely high-Q quasi-BICs induced by simultaneously broken out-of- and in-plane symmetries in dielectric metasurfaces of low-index materials. *Opt. Commun.* **2023**, *535*, 129356. [CrossRef]
35. Wang, J.; Niu, Y.; Zhang, M.; Wu, H.; Chen, J. Dual polarization-independent quasi-BICs enabled by out-of-plane symmetry breaking in nanodisk tetramer metasurface. *Opt. Lett.* **2025**, *50*, 5933–5936. [CrossRef] [PubMed]
36. Feng, J.; Wang, X.; Cheng, J.R.; Zeng, M. Polarization-independent bound state in the continuum without the help of rotational symmetry. *Opt. Lett.* **2023**, *48*, 4829–4832. [CrossRef] [PubMed]

Disclaimer/Publisher's Note: The statements, opinions and data contained in all publications are solely those of the individual author(s) and contributor(s) and not of MDPI and/or the editor(s). MDPI and/or the editor(s) disclaim responsibility for any injury to people or property resulting from any ideas, methods, instructions or products referred to in the content.